Chemical Physics 21 (1977) 327–347

N-METHYLMETHYLENEIMINE AND ETHYLIDENEIMINE: GAS- AND MATRIX-INFRARED SPECTRA, AB INITIO CALCULATIONS AND THERMODYNAMIC PROPERTIES

I. STOLKIN, T.-K. HA and Hs.H. GÜNTHARD
Laboratory for Physical Chemistry, Swiss Federal Institute of Technology, Universitätstrasse 22, CH-8006 Zurich, Switzerland

Received 3 November 1976

Gas- and matrix spectra of $CH_3N{:}CH_2$ (I) produced by controlled pyrolysis of N-trimethyl hexahydro-s-triazine and matrix spectra of $CH_3CH{:}NH$ (II) and its d_5 modification produced by photolysis in Ar matrices have been measured. A set of ab initio SCF LCAO calculations for both the cis and trans isomer of II, of I and of the isomers $CH_2{:}CHNH_2$ and CH_2NHCH_2 is given. For I and II assignments of the vibrational spectra, sets of harmonic force constants as well as statistical thermodynamic functions and thermodynamic data of their interconversion are presented.

1. Introduction

Alkylidene imines are generally considered to be unstable compounds with a pronounced tendency to polymerization and hydrolysis [1]. The lowest member of the series $CH_2{:}NH$ has first been studied by matrix isolation of the photo decomposition products of methyl azide [2] and diazomethane [3]. Recently its microwave spectrum has been measured by producing the molecule by high temperature pyrolysis of methylamine [4] and the study of photogenerated $CH_2{:}NH$ has been extended considerably by use of various isotopic species [5]. Also by using pyrolytic decomposition of ethylamine Lovas et al. [6] were able to identify the microwave spectrum of both geometrical isomers of the next higher homolog ethylideneimine (acetaldimine) and to derive information about its structure.

The interest in this class of compounds results from the lack of information on structural and thermochemical properties and from the possible use as highly reactive species in chemical reactions. The lower members probably occur in dust regions of space as has already been shown for $CH_2{:}NH$ [7].

In this paper we report the gas phase and matrix spectrum of the isomer $CH_3N{:}CH_2$ and the matrix spectra of the cis- and trans-isomers of ethylideneimine-d_0 and d_5. The latter molecules have been produced by photolysis of $CH_3CH_2N_3$, whereas the secondary imine was prepared by pyrolysis of N-trimethyl-hexahydro-s-triazine (NTMST) under well controlled conditions. The matrix spectra of the secondary imine and its d_3-modification had earlier been obtained by Curl et al. [8]. Both gas phase spectra (0.3 cm^{-1} resolution) and matrix spectra obtained in this work proved useful to correct the assignment proposed by these workers. Analysis of the vibrational spectra by normal coordinates is presented which will allow a fairly definite discrimination of the cis- and trans-isomer of the primary imine.

Besides the spectroscopic study a rather extended investigation of the 3 isomers by SCF ab initio quantum chemical calculations is reported. Based on both the quantum chemical and spectroscopic results a set of thermochemical data is given for the aliphatic primary and secondary imines with 2 carbon atoms.

2. Experimental

The imines studied in this work were synthesized either by thermal or photochemical decomposition.

2.1. Preparation of imines by thermal decomposition

Synthesis of $CH_3CH{:}NH$ and $CH_3N{:}CH_2$ had earlier been studied by thermal decomposition of aziridine (ethylideneimine) [9]. This process was carried out by the aid of a quartz wool catalyst in a temperature range between 400–550°C and was believed to lead to

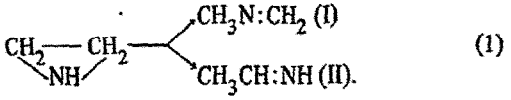

(1)

Besides the imines considerable amounts of NH_3 and more complex highly reactive imines were produced. It turned out to be difficult to select by catalytic decomposition either the secondary (I) or the primary imine (II). Only complex mixtures were obtained. These were found inconvenient for measurement of highly resolved spectra, in particular even traces on NH_3 hindered seriously determination and measurement of rotational structure of the absorption bands. Therefore, for generation of pure $CH_3N{:}CH_2$ the thermal decomposition (2) was used [10]

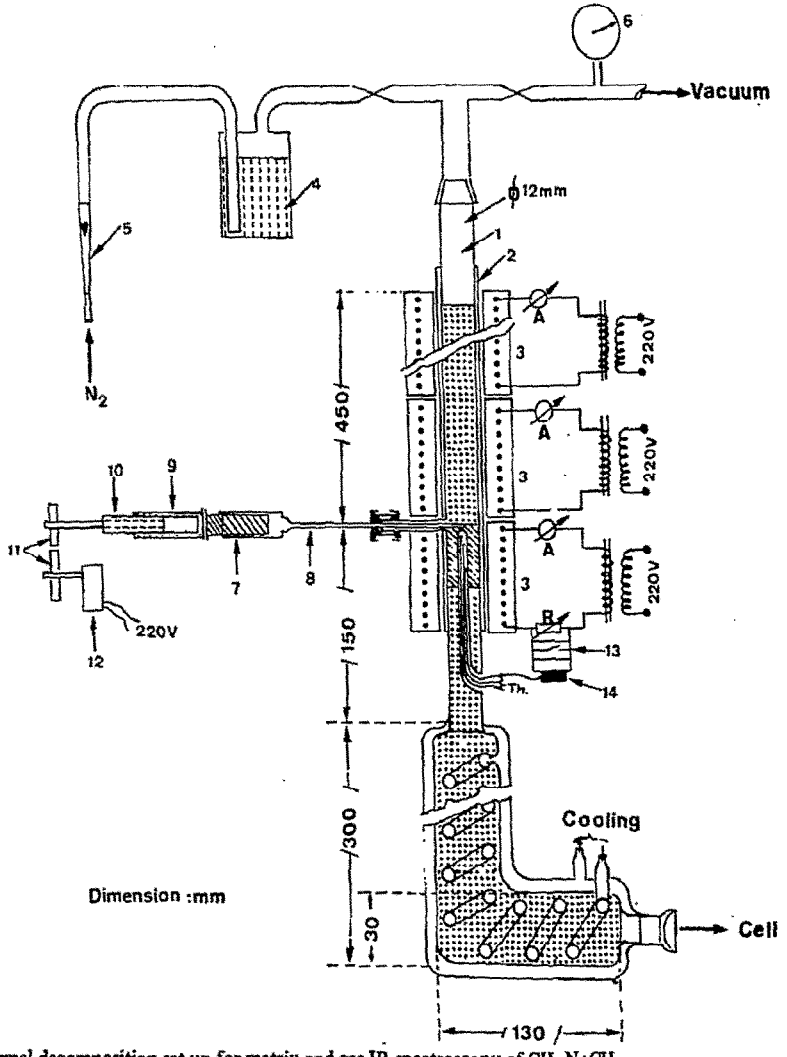

Fig. 1. Thermal decomposition set up for matrix and gas-IR-spectroscopy of $CH_3N{:}CH_2$.

Key: (1) reaction tube (pyrex), (2) copper tube, (3) electrical heater, (4) molecular sieve, (5) flow meter, (6) manometer, (7), (8) syringe with steel capillary, (9–12) drive for syringe, (13), (14) temperature control, (Th.) thermocouples.

Table 1
Operation conditions for catalytic thermal decomposition of NTMST

Parameter	Operation conditions
Carrier gas flow (N_2 or Ar)	21.5–85.3 cm^3/s (20°C, 720 torr)
NTMST molar fraction[a)]	5.6×10^{-3}
Catalyst	Mobil Oil 90% Al_2O_3, 10% SiO_2, 1 mm mesh
Catalyst height	25 mm
Catalyst temp.	350–400°C
Contact time (at 400°C and 720 torr)	0.01–0.001 s
Preheating zone	350–400°C
Cooling zone	−60–80°C

[a)] At injection point.

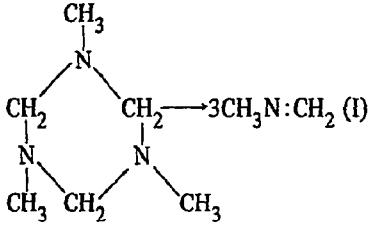

$$\rightarrow 3CH_3N{:}CH_2\ (I) \qquad (2)$$

N-trimethyl-hexahydro-s-triazine (NTMST).

Closer inspection of the chemical equilibrium [11] shows that thermal decomposition of NTMST requires well controlled conditions with respect to (w.r.t.) flow, temperature and contact time in order to obtain pure $CH_3N{:}CH_2$. The set up used in this work for measurement of the gas spectrum is schematically shown in fig. 1 [12] and served for measurement of both gas and matrix spectra. In order to achieve short residence times the flow of the carrier gas (N_2 or Ar) was controlled, furthermore the carrier gas was preheated in a packed zone of the reactor before entering the catalyst section. The reactant was injected by a motor driven syringe just in front of the latter and the gas steam effluent from it was cooled as fast as possible in a packed cooling section. Cooling temperatures between −60–−80°C were applied. Table 1 gives a view of the operation conditions of the reactor, these proved quite critical, if highly pure $CH_3N{:}CH_2$ should be obtained, in particular if NH_3 production is to be supressed. Presence of NH_3 renders gas spectra nearly useless. By optimization of the operating parameters it turned out possible to nearly completely suppress it and to observe the unobscured B type band of $CH_3N{:}CH_2$ at 952 cm^{-1}. Optimum operation conditions for pure $CH_3N{:}CH_2$ production were 350–380°C catalyst temperature and 7 ± 0.5 ms contact time. Prior to reaction the system was degassed for 24 h at 400°C and ≈ 5×10^{-3} torr.

Experiments for preparation of $CH_3CH{:}NH$ by thermal decomposition of aziridine (1) or of C-trimethyl-hexhydro-s-triazine (CTMST) (2')

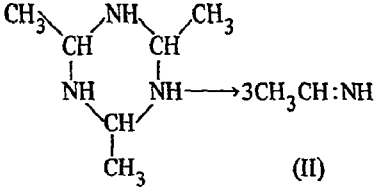

$$\rightarrow 3CH_3CH{:}NH \qquad (2')$$

(II)

were carried out in the same set up, fig. 1, though the injection device had to be replaced by a thermostat controlled carrier gas saturator filled with solid CTMST. Neither with quartz wool nor with alumina silica catalyst in the temperature range 370–535°C and residence time of 0.007–0.014 s could the formation of NH_3 from aziridine be suppressed. Thermal decomposition of CTMST under similar conditions again did not yield the imine in sufficient yield and purity. As a consequence no gas spectrum of the primary imine could be obtained.

2.2. *Preparation of imines of photolysis*

For photolysis of ethylazide in Ar matrices at LHe temperature the azide was deposited together with the matrix gas (M/A ratios 500–2500) onto a CsI window. Photolysis was effectuated by a Xe arc pressure lamp XBO 1600 (Osram), whose output was directed through a lens system including a 20 cm H_2O infrared filter towards the target of the cryostat with the latter placed in the spectrometer. Irradiation times were adjusted by observation of the vanishing matrix spectrum of the azide; 3–7 h had to be applied usually.

2.3. *Chemicals*

NTMST and CTMST were prepared along procedures

described in literature [13]. NTMST was purified prior to use by 3 destillations in a spinning band column (30 ETP) and stored over outgassed molecular sieve 4A. Preparation of ethylazide followed a procedure reported by Staudinger [14]; purification was effected by distillation through a spinning band column. GC analysis of the sample yielded $\leqslant 0.3\%$ total impurities. For storage the azide was condensed into breakoff seal ampoules.

Ethylazide-d_5 was prepared by the same overall procedure; the diethyl sulfate-d_{10} required in the first step was made by dropwise addition of D_2SO_4 ($\geqslant 90\%$ D *) to ethanol-d_6 ** at $-8,\ldots,-1$°C and distillation of the reaction mixture at 6 torr and 35–45°C. No further purification of the diethylsulfate-d_{10} so obtained was made prior to its use for the reaction with sodium azide $(C_2D_5)_2SO_4 + 2NaN_3 \rightarrow 2C_2D_5N_3 + Na_2SO_4$.

* Chemie Uetikon.
** Merck, Sharp and Döhme.

2.4. Instrumentation

Gas spectra were taken with a Perkin-Elmer Model 225 spectrophotometer equipped with a 1 m gas cell of our own design. The cell was combined with the reactor system fig. 1, to form a flow system, thereby allowing the measurement of gas spectra with high resolution and long time constants. Molar fraction of imine in the flow was kept below 10^{-2} to avoid polymerization. Spectral slit widths between 2 cm^{-1} (for overall spectra) and 0.2 cm^{-1} (for measurements of rotational fine structure) were applied. In the latter case it proved necessary to scan particular bands repeatedly and to pool and average up to 10 spectra.

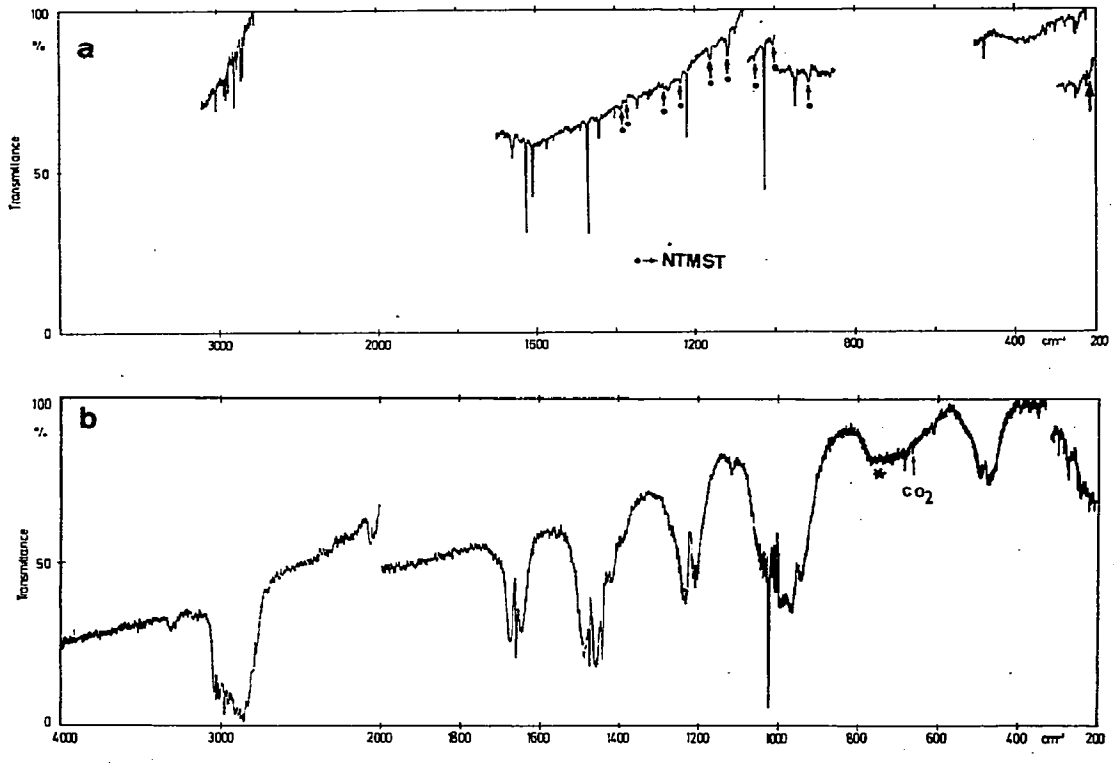

Fig. 2. Matrix- and gas-infrared spectra of $CH_3N{:}CH_2$ (I).
(a) $CH_3N{=}CH_2$: Ar(s) M/A ≈ 2500, LHe temperature, slit program 4. Bands marked with • originate from NTMST. In sections without recorder trace no bands of (I) were found.
(b) $CH_3N{=}CH_2$(g) : l = 1 m, $p \leqslant 6$ torr, $x \leqslant 8 \times 10^{-3}$, slit program 4. Bands marked with *: cell absorption.

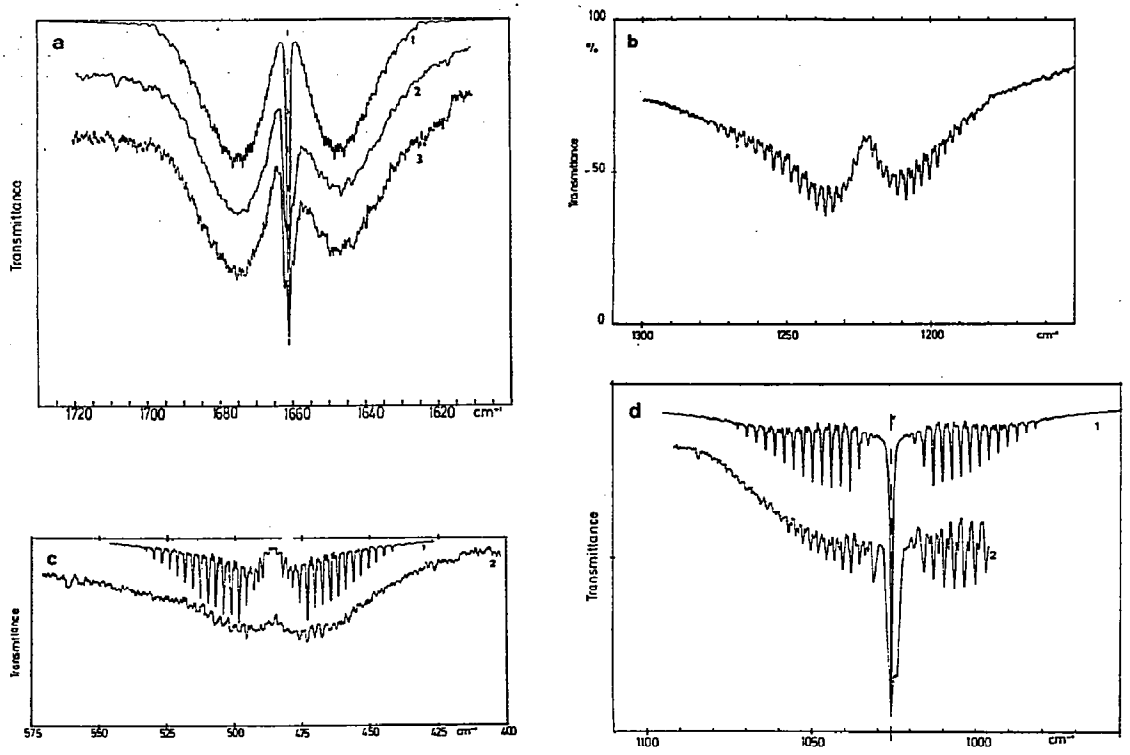

Fig. 3. Rotational structure of rotation–vibration bands of $CH_3N:CH_2$ (g), 1 m path length, total pressure 720 torr, molar fraction $\leq 8 \cdot 10^{-3}$

(a) A–B hybrid type band $\nu_5{}^{\nu}(C{=}N)(a')$, 1661 cm^{-1}, spectral slit width 0.3 cm^{-1}. (1) Computed envelope 90% A-type, 10% B-type; (2) signal averaged band from 8 single scans; (3) single scan measurement.

(b) B-type band $\nu_9(a')$, 1220 cm^{-1}, spectral slit width 0.5 cm^{-1}.

(c) B-type band $\nu_{12}{}^{\delta}(CN{:}C)(a')$, 484 cm^{-1}. (1) Computed envelope; (2) experimental band, spectral slit width 0.6 cm^{-1}.

(d) C-type band, $\nu_{16}{}^{\gamma_t}(CH_2)(a'')$, 1026 cm^{-1}. (1) Computed envelope; (2) experimental band, spectral slit width 0.5 cm^{-1}.

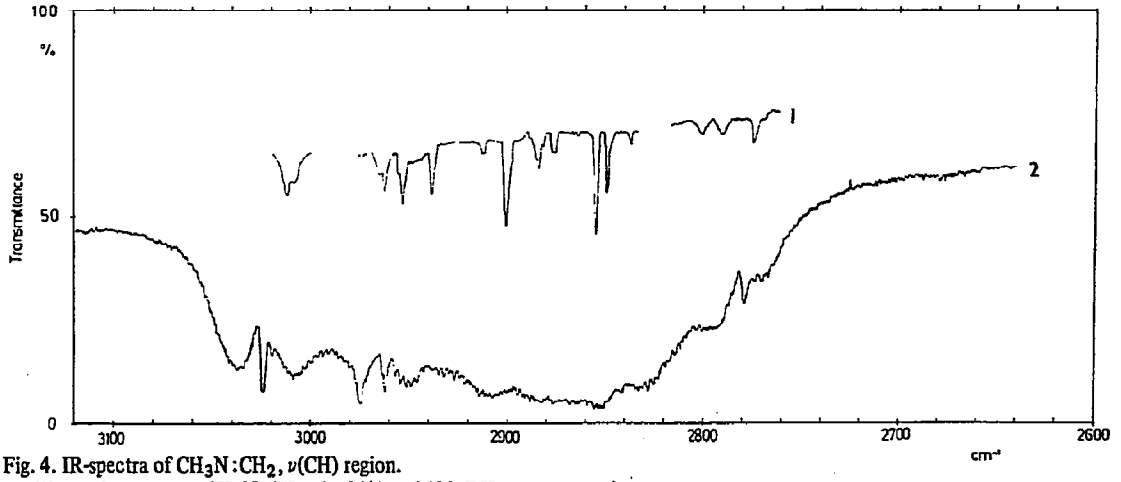

Fig. 4. IR-spectra of $CH_3N:CH_2$, ν(CH) region.

(1) matrix spectrum $CH_3N:CH_2:Ar$, M/A ≈ 2500 (LHe temperature).

(2) Gas-phase spectrum, total pressure 720 torr, molar fraction $\leq 8 \times 10^{-3}$, spectral slit width 0.9–1.2 cm^{-1}.

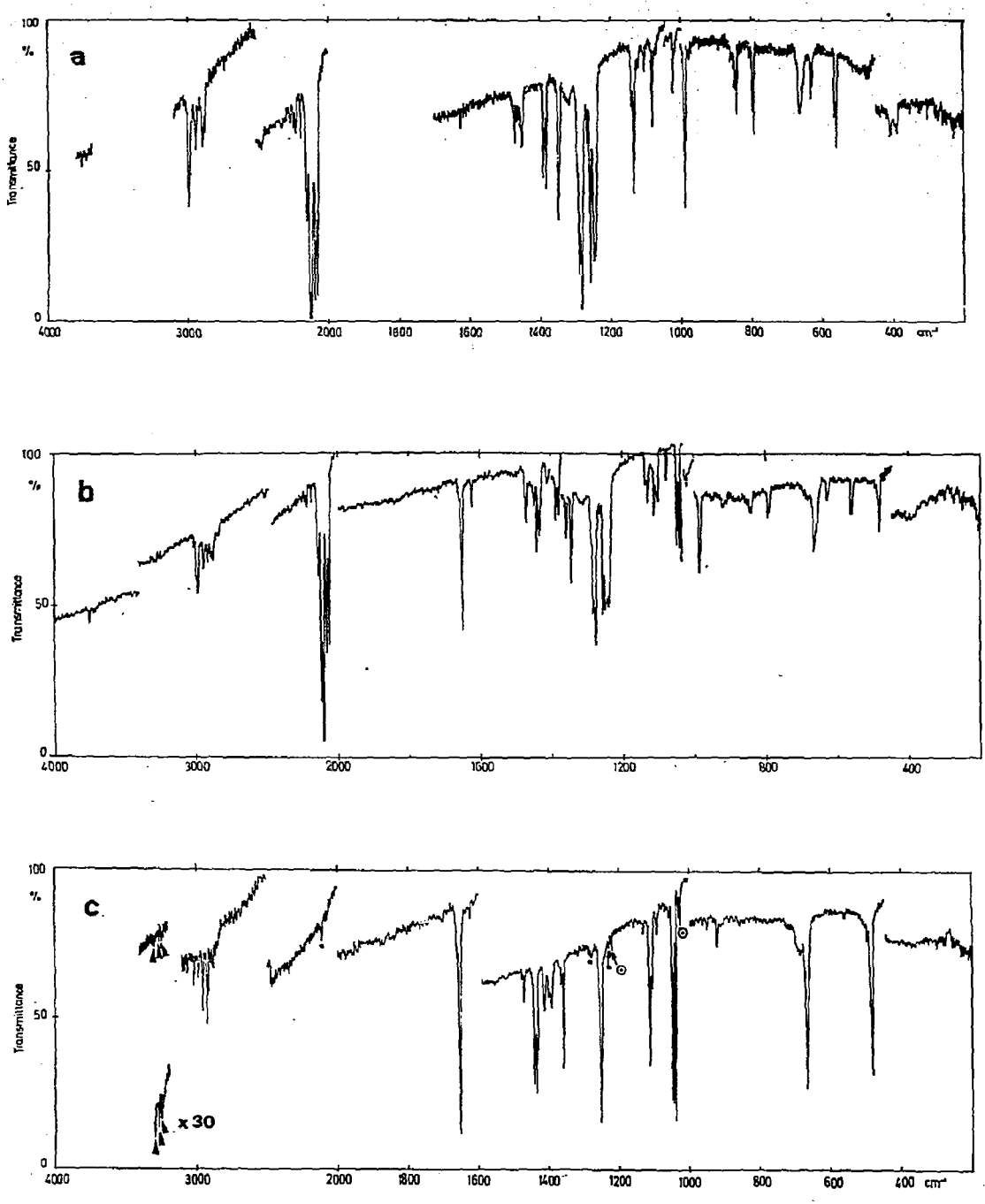

Fig. 5. Photolysis of $CH_3CH_2N_3$: Ar(s), matrix spectra of $CH_3CH_2N_3$, CH_3CH : NH, M/A ≈ 2500 (LHe temperature), slit program 4. *Key*: (a) $CH_3CH_2N_3$: Ar, before irradiation; (b) after 45 min irradiation; (c) after 180 min irradiation. (▲): NH-stretching region, 30 X ordinate expansion. (●): $CH_3CH_2N_3$ bands. (⊖): CH_3N : CH_2 bands.

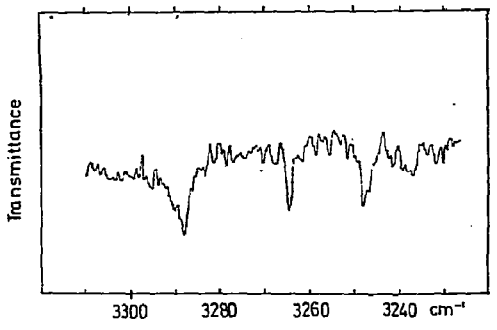

Fig. 6. Spectrum of $CH_3CH:NH:Ar$ ν(NH) region, LHe temperature, M/A ≈ 2500, slit program 4; 30 fold ordinate expansion.

Matrix spectra were taken with a Perkin-Elmer Model 325 spectrophotometer combined with a LHe cryostat of our own design [15]. The cryostat was directly connected to the output of the cooling section of the reactor fig. 1. The reactor output was sampled by a Knudsen type orifice. The molecular beam effusing from it was codeposited with an Ar molecular beam in order to control the M/A ratio in the range 500–2500 *. Deposition rates were measured with a small laser [16], usually layer growth rates of 1–2 μm/min and layer thicknesses of 100–600 μm were applied.

* M/A ratio: (molar fraction)$^{-1}$.

3. Experimental results

In fig. 2 overall gas and matrix spectra of $CH_3N:CH_2$ are reproduced. A number of particular absorption bands taken with the higher resolving power available in this work are shown in fig. 3 together with computed band evelopes. The ν(CH) region of $CH_3N:CH_2$ spectra taken with higher resolution is shown in fig. 4, which documents the complications produced (at least in part) by Fermi resonance.

The matrix spectra of ethylazide and of the photoproducts growing from the azide under irradiation are shown in fig. 5. Expanded sections of the matrix spectrum of the photoproducts are reproduced in figs. 6 and 7; the former showing the ν(N–H) region taken with 30-fold ordinate expansion, the latter documenting regions where the presence of trans- and cis-isomers of ethylideneimine leads to typical splitting patterns.

A set of two matrix spectra observed before and after the photolysis of $CD_3CD_2N_3$ is given by fig. 8. The photoprocesses of d_0- and d_5-species appear to proceed in the same way within the detectability limits

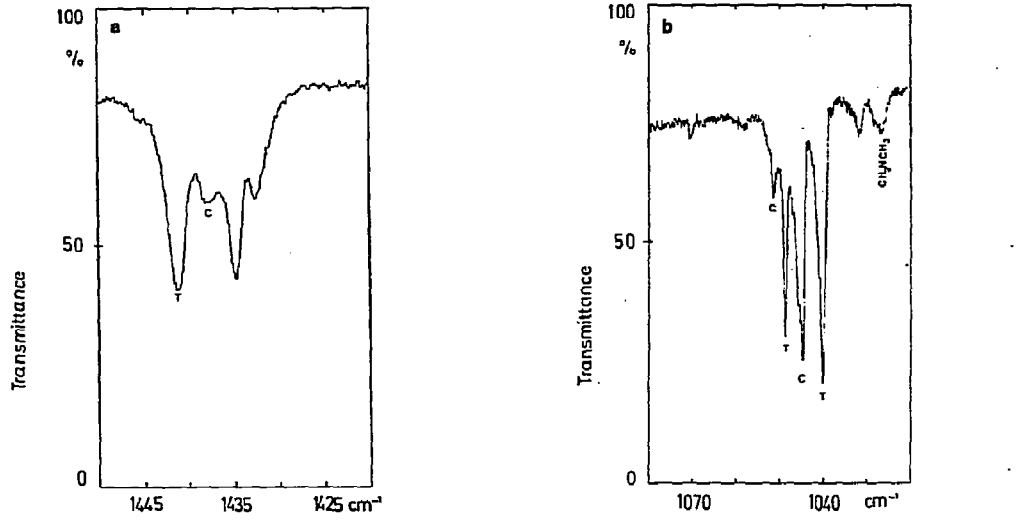

Fig. 7. Spectrum of $CH_3CH:NH:Ar(s)$, M/A ≈ 2500, LHe temperature, slit program 4. (a) $\delta(CH_3)$ region; (b) $\gamma_\perp$(CH) – δ(C:NH) region; T(C): bands attributed to trans (cis) isomer.

Table 9
CH_3CH:NH structural parameters, internal coordinates and valence force constants (cf. fig. 14)

Structural [a] parameters			Internal [b] coordinates	Force constant	
	cis	trans		cis	trans
S_1	1.016	1.020	R_1^I	5.75(13)	5.891(32)
r_4, r_5, r_6	1.089	1.089	R_2^I, R_3^I, R_4^I	4.767(33)	4.728(23)
d	1.114	1.114	R_5^I	4.692(60)	4.656(29)
D	1.345	1.324	R_6^I	9.11(58)	9.432(16)
S_2	1.54	1.54	R_7^I	5.31(55)	4.92(27)
α_4, α_5, α_6	109.5	109.5	$R_8^{II}, R_9^{II}, R_{10}^{II}$	0.515(11)	0.518(5)
β_4, β_5, β_6	109.5	109.5	$R_{11}^{II}, R_{12}^{II}, R_{13}^{II}$	0.670(25)	0.638(15)
θ_1	113	247	R_{14}^{II}	0.627(40)	0.705(5)
ζ	0.5		R_{15}^{III}	1.039(95)	0.862(42)
γ_1			$R_{16}^{IV}(H_7C_2N_1C_3)$	0.308(25)	0.240(11)
θ_2	124	124	R_{17}^{II}	1.58(32)	1.916(10)
τ			$R_{18}^{V}(N_1C_2C_3H_{7,8})$	0.454(28)	0.463(8)
τ			$R_{19}^{V}(N_1C_2C_3H_{4,5,6})$ $(H_7C_2C_3H_{4,5,6})$	0.05	0.05
			R_2^I, R_3^I		0.147(49)
			R_7^I, R_8^{II}	−0.28(18)	−0.241(30)
			R_7^I, R_{15}^{III}		−0.668(85)
			R_8^{II}, R_{12}^{II}		0.022(9)
			$R_{17}^{II}, R_{15}^{III}$		−0.488(47)
			R_{11}^{II}, R_{17}^{II}	−0.31(17)	
			R_1^I, R_6^I	−1.37(46)	

[a] Bond length in A, bond angles in degrees, values used for ab initio calculation, for definition see fig. 13 and section 4.
[b] For definition cf. ref. [12] and fig. 13.

very weak in related molecules CH_3N:NH [31], CH_2:NH [5] considerable effort has been made to detect this mode. Use of ordinate expansion (30X) finally yielded reproducibly the spectra in figs. 6 and 9, respectively, which support rather definitely the presence of ν(NH) and ν(ND) bands. For (II-d_0) 3 bands in the range 3300–3200 cm^{-1} are observed, which have been attributed to $t\tilde{\nu}_1$(NH)(a′) (3264 cm^{-1}), $c\tilde{\nu}_1$(NH)(a′) (3247 cm^{-1}) and to $c2\tilde{\nu}_5$ (a′) (3288 cm^{-1}). For (II-d_5) the same region exhibits a single band near 3317 cm^{-1} of unknown origin, but it may be interpreted as a combination tone. In the 2500–2400 cm^{-1} region two bands are observed at 2452 cm^{-1}, $t\tilde{\nu}_1$ (a′) and 2425 cm^{-1}, $c\tilde{\nu}_1$ (a′), which may be considered as ν(ND) modes.

(ii) The ν(CH) – ν(CD) isotope shifts behave similarly to related molecules like CH_3CH:NCH_3 [29], CH_3CHO [30].

(iii) The ν(C:N)-region of (II-d_5) exhibits 6 bands, which may be grouped into site doublets at 1631/1628 and 1615/1613 cm^{-1} attributed to the fundamentals $c\nu_5$(a′), $t\nu_5$(a′) and to combination bands, respectively.

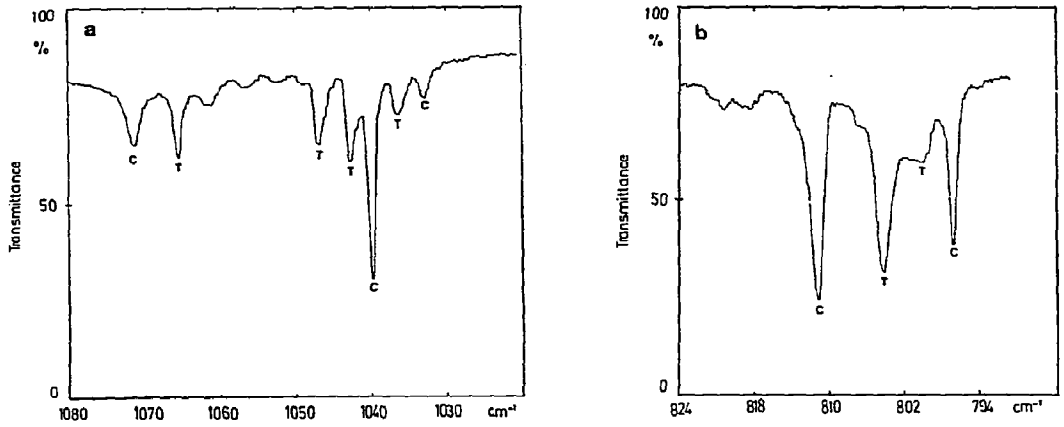

Fig. 10. IR-spectrum of CD_3CD:ND:Ar(s), LHe temperature, M/A ≈ 2500, slit program 4. (a) $\delta(CD_3)$ region; (b) $\gamma_{\parallel}(CD_3) - \gamma_{\perp}(CD_3)$ region; T(C): bands attributed to trans (cis) isomer.

Table 2
CH_3N:CH_2 gas- and matrix-infrared spectrum

Frequency (cm^{-1})				Assignment	Approximate mode description (PED)
Gas	Band env.	Ar-matrix	calc.		
3308(w)				$2\tilde{\nu}_5(A')$	
3024(s)	AB	3012(s)	3015	$\tilde{\nu}_1(a')$	$\nu_a(CH_2)(100)$
3020(w)		3011(w)			
2975(s)	C	2962(ms)	2967	$\tilde{\nu}_{13}(a'')$	$\nu_a(CH_3)(100)$
2962(s)	AB	2953(s)	2969	$\tilde{\nu}_2(a')$	$\nu_a(CH_3)(99)$
2940?	B	2938(s)	2896	Fermi-reson. $2\tilde{\nu}_6(A')$	$\nu_s(CH_2)(99)$
2897(w)		2900(s)		$\tilde{\nu}_3(a')$	
		2884(ms)		Fermi-reson. $2\tilde{\nu}_7(A'), 2\tilde{\nu}_{14}(A')$	
		2876(w)			
2841?	AB	2838(w)		$\tilde{\nu}_7 + \tilde{\nu}_8(A')$	$\nu_s(CH_3)(100)$
2779?		2774(m)		$2\tilde{\nu}_8(A')$	
		2854(s)	2850		
		2849(s)		$\tilde{\nu}_4(a')$	
2053(w)		2050(w)		$2\tilde{\nu}_{16}(A')$	
1678(w)		1678(w)		$\tilde{\nu}_{14} + \tilde{\nu}_{18}(A')$	
1661(s)	AB	1659(m)	1659	$\tilde{\nu}_5(a')$	$\nu(C{=}N)(73) + \delta(CH_2)(29)$
1475(vs)	AB	1470(vvs)	1469	$\tilde{\nu}_6(a')$	$\delta(CH_2)(55) - \delta_a(CH_3)(19) - \gamma_{\parallel}(CH_3)(10)$
		1473?(vw)			
				$\tilde{\nu}_7(a')$	
		1442(vw)	1443	or	$\delta_a(CH_3)(62) + \delta(CH_2)(16) + \gamma_{\parallel}(CH_3)(7)$
				$\tilde{\nu}_{10} + \tilde{\nu}_{12}(A')$	
1444(s)	C	1441(m)	1447	$\tilde{\nu}_{14}(a'')$	$\delta_a(CH_3)(85) + \gamma_{\perp}(CH_3)(15)$
				$\tilde{\nu}_{10} + \tilde{\nu}_{12}(A')$	
1425(w)	B			or	see above
				$\tilde{\nu}_7(a')$	

Continued on next page.

Table 2 (continued)

Frequency (cm^{-1})				Assignment	Approximate mode description (PED)
Gas	Band env.	Ar-matrix	calc.		
1405(vw)	AB	1402(m)	1403	$\tilde{\nu}_8(a')$	$\delta_s(CH_3)(100)$
1220(s)	B	1221(s)	1210	$\tilde{\nu}_9(a')$	$\gamma_{\parallel}(CH_3)(37) + \nu(N-C)(29) - \delta_a(CH_3)(15) - \delta(CNC)(10)$
		1100(vw)	1130	$\tilde{\nu}_{15}(a'')$	$\gamma_{\perp}(CH_3)(74) - \delta_a(CH_3)(13) - \gamma_{\perp}(CH_2)(7) + \tau(C=N)(5)$
1026(vs)	C	1026(vvs)	1031	$\tilde{\nu}_{16}(a'')$	$\gamma_{\perp}(CH_2)(90) + \gamma_{\perp}(CH_3)(8)$
952(m)	B	950(ms)	960	$\tilde{\nu}_{10}(a')$	$\nu(N-C)(47) - \gamma_{\parallel}(CH_3)(36) + \gamma_{\parallel}(CH_2)(31)$
			883	$\tilde{\nu}_{11}(a')$	$\gamma_{\parallel}(CH_2)(51) - \nu(N-C)(32)$
686(w)	C		689	$\tilde{\nu}_{17}(a'')$	$\tau(C=N)(94)$
484(ms)	B	479(ms)	488	$\tilde{\nu}_{12}(a')$	$\delta(CNC)(90) + \gamma_{\parallel}(CH_3)(10) + \gamma_{\parallel}(CH_2)(11)$
		220?(w)	212	$\tilde{\nu}_{18}(a'')$	$\tau(CH_3)(99)$

Table 3
cis-CH_3CH:NH and trans-CH_3CH:NH matrix-infrared spectra

Frequency (cm^{-1})		Assignment c: cis t: trans	Approximate mode description (PED)
obs. Ar-matrix	calc.		
3288(vvw)		c $2\tilde{\nu}_5(A')$	
3264(vvw)	3270	t $\tilde{\nu}_1(a')$	$\nu(NH)(95)$
3247(vvw)	3266	c $\tilde{\nu}_1(a')$	$\nu(NH)(100)$
3060(vw)		c $\tilde{\nu}_7 + \tilde{\nu}_5(A')$	
3018(m)	3018	c $\tilde{\nu}_2(a')$	$\nu_a(CH_3)(96)$
	2997	t $\tilde{\nu}_2(a')$	$\nu_a(CH_3)(98)$
2990(m)	2982	c $\tilde{\nu}_{13}(a'')$	$\nu_a(CH_3)(99)$
	2994	t $\tilde{\nu}_{13}(a'')$	$\nu_a(CH_3)(99)$
2954(ms)	2940	t $\tilde{\nu}_3(a')$	$\nu(CH)(97)$
2925(m-s) 2920(m)	2931	c $\tilde{\nu}_3(a')$	$\nu(CH)(98)$
2885(m)	2878	t $\tilde{\nu}_4(a')$	$\nu_s(CH_3)(97)$
	2878	c $\tilde{\nu}_4(a')$	$\nu_s(CH_3)(99)$
1659(sh)	1677	t $\tilde{\nu}_5(a')$	$\nu(C=N)(61) - \nu(CC)(18) - \gamma_{\parallel}(CH)(18)$
1652(vs)	1655	c $\tilde{\nu}_5(a')$	$\nu(C=N)(81) - \nu(CC)(11)$
1438(ms)	1440	c $\tilde{\nu}_6(a')$	$\delta_a(CH_3)(93) - \gamma_{\parallel}(CH_3)(7)$
1435(s) 1433(s)	1441	c $\tilde{\nu}_{14}(a'')$	$\delta_a(CH_3)(92) + \gamma_{\perp}(CH_3)(8)$
1435(s) 1433(s)	1439	t $\tilde{\nu}_{14}(a'')$	$\delta_a(CH_3)(91) + \gamma_{\perp}(CH_3)(9)$
1412(m)	1410	c $\tilde{\nu}_7(a')$	$\delta_s(CH_3)(97)$
1398(w-m) 1392(m)	1406	t $\tilde{\nu}_7(a')$	$\delta_s(CH_3)(81)$
1365(w)		t $2\tilde{\nu}_{17}(A')$	

Table 3 (continued)

Frequency (cm^{-1}) obs. Ar-matrix	calc.	Assignment c: cis t: trans	Approximate mode description (PED)
1358(s)	1328	t $\tilde{\nu}_8$(a')	δ(CNH)(21) − $\gamma_{\parallel}$(CH)(19) − ν(CC)(12) + δ_a(CH_3)(12) + δ(NCC)(10)
1252(vs)	1258	c $\tilde{\nu}_8$(a')	δ(CNH)(36) + $\gamma_{\parallel}$(CH)(15) − δ(NCC)(19) + ν(C=N)(7) + $\gamma_{\parallel}$(CH_3)(8) + ν(CC)(7)
1160(vw)	1185	t $\tilde{\nu}_{15}$(a'')	τ(C=N)(69) − $\gamma_{\perp}$(CH)(26)
1132(vw)	1124	c $\tilde{\nu}_{15}$(a'')	τ(C=N)(93) − $\gamma_{\perp}$(CH)(6)
1114(ms)	1114	c $\tilde{\nu}_9$(a')	$\gamma_{\parallel}$(CH)(62) − δ(CNH)(11) − ν(CC)(7)
1106(ms-s)	1100	t $\tilde{\nu}_9$(a')	$\gamma_{\parallel}$(CH)(62) − ν(CC)(26)
1052(w-m)	1050	c $\tilde{\nu}_{10}$(a')	−δ(CNH)(44) + ν(CC)(35) + $\gamma_{\parallel}$(CH_3)(13)
1045(vs)	1045	c $\tilde{\nu}_{16}$(a'')	$\gamma_{\perp}$(CH_3)(78) − $\gamma_{\perp}$(CH)(9) − δ_a(CH_3)(7)
1040(s)	1061	t $\tilde{\nu}_{10}$(a')	δ(CNH)(47) + $\gamma_{\parallel}$(CH_3)(42)
	1036	t $\tilde{\nu}_{16}$(a'')	$\gamma_{\perp}$(CH_3)(81) − τ(C=N)(10) − δ_a(CH_3)(7)
962(w)		c $2\tilde{\nu}_{12}$(A')	
950(w)	947	c $\tilde{\nu}_{11}$(a')	$\gamma_{\parallel}$(CH_3)(64) + ν(CC)(25)
920(w-m)	920	t $\tilde{\nu}_{11}$(a')	ν(CC)(39) + δ(CNH)(25) + ν(C=N)(18) − $\gamma_{\parallel}$(CH_3)(16)
674(w)	669	c $\tilde{\nu}_{17}$(a'')	$\gamma_{\perp}$(CH)(83) + $\gamma_{\perp}$(CH_3)(11)
668(s)	681	t $\tilde{\nu}_{17}$(a'')	$\gamma_{\perp}$(CH)(71) + τ(C=N)(21)
498(w-m)	492	t $\tilde{\nu}_{12}$(a')	δ(NCC)(91) + $\gamma_{\parallel}$(CH_3)(24)
485(s)	483	c $\tilde{\nu}_{12}$(a')	δ(NCC)(93) + $\gamma_{\parallel}$(CH)(42) + ν(CC)(23)
	193	t $\tilde{\nu}_{18}$(a'')	τ(CH_3)(98)
	187	c $\tilde{\nu}_{18}$(a'')	τ(CH_3)(98)

Table 4
cis-CD_3CD:ND and trans-CD_3CD:ND matrix-infrared spectra

Frequency (cm^{-1}) obs. Ar-matrix	calc.	Assignment c: cis t: trans	Approximate mode description (PED)
3317(vvw)		t $\tilde{\nu}_2 + \tilde{\nu}_7$(A')	
2452(vvw)	2445	t $\tilde{\nu}_1$(a')	ν(ND)(84)
2425(vvw)	2399	c $\tilde{\nu}_1$(a')	ν(ND)(97)
2256(m-w)	2254	c $\tilde{\nu}_2$(a')	ν_a(CD_3)(93)
2243(m-w)	2245	t $\tilde{\nu}_2$(a')	ν_a(CD_3)(89) + ν(CD)(7)
	2233	t $\tilde{\nu}_{13}$(a'')	ν_a(CD_3)(98)
2216(m-w)	2224	c $\tilde{\nu}_{13}$(a'')	ν_a(CD_3)(98)
2209(m-w)	2186	t $\tilde{\nu}_3$(a')	ν(CD)(85)
2191(m)	2183	c $\tilde{\nu}_3$(a')	ν(CD)(89)
2184(vw)		t $\tilde{\nu}_6 + \tilde{\nu}_{15}$	
2062(w)	2077	c $\tilde{\nu}_4$(a')	ν_s(CD_3)(97)
2058(w)	2078	t $\tilde{\nu}_4$(a')	ν_s(CD_3)(96)
1696(w)		t $2\tilde{\nu}_9$(A')	

Continued on next page

Table 4 (continued)

Frequency (cm^{-1}) obs. Ar-matrix	calc.	Assignment c: cis t: trans	Approximate mode description (PED)
1636(w)		t $2\tilde{\nu}_{17} + \tilde{\nu}_{11}$(A')	
1631(s) } 1628(vs) }	1629	c $\tilde{\nu}_5$(a')	ν(C=N)(80) − ν(CC)(13)
1621(vw)		c $2\tilde{\nu}_{16}$(A')	
1615(w)		t $2\tilde{\nu}_{10}$(A')	
1613(m)	1602	t $\tilde{\nu}_5$(a')	ν(C=N)(65) − ν(CC)(19) + ν(ND)(13)
1205(w)		c $\tilde{\nu}_{10} + \tilde{\nu}_{12}$(A')	
1200(m)	1212	t $\tilde{\nu}_6$(a')	ν(CC)(41) + $\delta_s(CD_3)$(16) − δ(CND)(12) − δ(NCC)(10) + ν(C=N)(10)
1159(ms)	1159	c $\tilde{\nu}_6$(a')	ν(CC)(47) − $\delta_s(CD_3)$(49)
1139(w)		c $\tilde{\nu}_{11} + \tilde{\nu}_{12}$(A')	
1072(m)	1066	c $\tilde{\nu}_7$(a')	$-\delta_s(CD_3)$(25) + δ(CND)(15) − δ(NCC)(21) + $\delta_a(CD_3)$(12) + $\gamma_{\parallel}$(CD)(9)
1065(m)	1063	t $\tilde{\nu}_7$(a')	$\delta_s(CD_3)$(73)
1046(m)	1034	t $\tilde{\nu}_{14}$(a'')	$\delta_a(CD_3)$(94)
1042(m)	1033	t $\tilde{\nu}_8$(a')	$\delta_a(CD_3)$(94)
1039(s)	1036	c $\tilde{\nu}_{14}$(a'')	$\delta_a(CD_3)$(95)
1032(w-m)	1033	c $\tilde{\nu}_8$(a')	$\delta_a(CD_3)$(83) + $\gamma_{\parallel}(CD_3)$(7)
986(m)	926	t $\tilde{\nu}_{15}$(a'')	τ(C=N)(43) − $\gamma_{\perp}$(CD)(39) + $\gamma_{\perp}(CD_3)$(15)
850(w)	851	c $\tilde{\nu}_9$(a')	δ(CND)(26) − ν(CC)(28) + $\delta_s(CD_3)$(24)
848(m-s)	854 t $\tilde{\nu}_9$(a')		$\gamma_{\parallel}$(CD)(56) − $\gamma_{\parallel}(CD_3)$(26) − δ(CND)(10)
	848 c $\tilde{\nu}_{15}$(a'')		$\gamma_{\perp}(CD_3)$(62) − $\gamma_{\perp}$(CD)(15) + τ(C=N)(16)
821(vw)		t $2\tilde{\nu}_{12}$(A')	
818(vw)		c $2\tilde{\nu}_{12}$(A')	
811(s)	822	c $\tilde{\nu}_{16}$(a'')	τ(C=N)(81) − $\gamma_{\perp}$(CD)(10)
804(s)	807	t $\tilde{\nu}_{10}$(a')	$\gamma_{\parallel}(CD_3)$(31) + $\gamma_{\parallel}$(CD)(22) − ν(CC)(19)
799(m-w)	799	t $\tilde{\nu}_{16}$(a'')	$\gamma_{\perp}(CD_3)$(65) − τ(C=N)(32)
796(s)	793	c $\tilde{\nu}_{10}$(a')	$\gamma_{\parallel}$(CD)(68) − δ(CND)(35)
736(m)	740 c $\tilde{\nu}_{11}$(a')		$\gamma_{\parallel}(CD_3)$(76) + δ(CND)(10)
	723 t $\tilde{\nu}_{11}$(a')		δ(CND)(61) + ν(CC)(12) + ν(C=N)(12)
527(m)	533	c $\tilde{\nu}_{17}$(a'')	$\gamma_{\perp}$(CD)(74) + $\gamma_{\perp}(CD_3)$(28)
495(vs)	521	t $\tilde{\nu}_{17}$(a'')	$\gamma_{\perp}$(CD)(60) + τ(C=N)(24) + $\gamma_{\perp}(CD_3)$(15)
411(s)	420	t $\tilde{\nu}_{12}$(a'')	τ(NCC)(83) + $\gamma_{\parallel}(CD_3)$(37)
405(m)	407	c $\tilde{\nu}_{12}$(a')	δ(NCC)(84) + $\gamma_{\parallel}$(CD)(44) + ν(CC)(17)
n.o.	146	t $\tilde{\nu}_{18}$(a'')	$\tau(CD_3)$(99)
n.o.	138	c $\tilde{\nu}_{18}$(a'')	$\tau(CD_3)$(99)

(i) relative stability of the two geometrical isomers

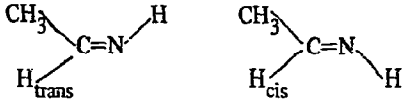

(ii) barrier to the methyl group rotation;

(iii) barrier to inversion of the NH group, i.e., the barrier to interconversion of trans and cis via in-plane inversion of the NH group;

(iv) barrier to internal rotation of the C=N double bond.

Furthermore, from quantum chemical calculations one may expect to obtain information about the r_e structural parameters r_e(C=N), r_e(NH) and $\measuredangle_e$(CNH) of both cis and trans isomers of acetaldimine (II).

For ab initio calculations we have employed approximate Hartree–Fock atomic SCF orbitals of the gaussian lobe functions [17]. The basis set consists of three contractions of 4, 3 and 3 gaussians for s orbitals and one contraction of 5 pairs of gaussian lobes for the three p orbitals of carbon and nitrogen, respectively. Each hydrogen s orbital is represented by one contraction of 5 gaussians [18], scaled by a factor of $2^{1/2}$ for the molecular calculation. Previously, we had adopted this size of the atomic double-zeta quality basis set for the calculations of rotational barriers in glyoxal [19] nitroethylene [20] and methylamine [21], for the study of internal H bonding and conformation of ethylene glycol [22] and for the study of the barrier to proton tunnelling in acetic acid monomer [23].

Ground state energy calculations were carried out as a function of some of the structural parameters in order to obtain partially optimized structures. The optimization process was started with the distance r(C=N) for the trans isomer. At the minimum of E_t w.r.t. r(C=N), the distance r(N–H) and the angle $\tau = \measuredangle$(CNH) were successively optimized. This procedure yielded partially optimized structural parameters:

r'_e(C=N) = 1.33 Å, r'_e(N–H) = 1.02 Å,

$\tau'_e(\measuredangle(\mathrm{CNH})) = 112.8°$.

In the partial optimization the experimental structural parameters of $CH_3CH{:}CH_2$ for the CH_3CH: fragment were used.

A similar optimization was carried out for the cis-isomer and yielded the following results:

Table 5
Molecular energies in ethylideneimine [a]

	trans	cis
E_T [b]	−132.8978	−132.8951
E_K [c]	132.3390	132.3384
E_N [d]	69.2040	68.8927
Orbital energies	−15.5704 (1a)	−15.5683 (1a)
	−11.3837 (2a)	−11.3804 (2a)
	−11.2823 (3a)	−11.2761 (3a)
	−1.1908 (4a)	−1.1901 (4a)
	−0.9973 (5a)	−0.9924 (5a)
	−0.8141 (6a)	−0.7947 (6a)
	−0.6359 (7a)	−0.6805 (7a)
	−0.6223 (8a)	−0.5905 (1b)
	−0.6004 (1b)	−0.5656 (8a)
	−0.5487 (9a)	−0.5513 (9a)
	−0.4225 (2b)	−0.4216 (2b)
	−0.4156 (10a)	−0.4162 (10a)

[a] Atomic units.
[b] Total molecular SCF energy.
[c] Kinetic energy of electrons.
[d] Nuclear–nuclear repulsion energy.

r'_e(C=N) = 1.35 Å, r'_e(N–H) = 1.01 Å,

$\tau'_e(\measuredangle(\mathrm{CNH})) = 112.5°$.

In both optimizations the conformation of the methyl group was held constant with the methyl group staggering the C=N double bond.

Table 5 summarizes (partially optimized) molecular energies for both geometrical isomers of ethylidene imine. The dipole moment of the trans isomer is calculated as 2.72 D. The trans isomer turns out to be more stable.

Table 6 summarizes relative energies of the various isomers and conformers w.r.t. t-$CH_3CH{:}NH$. The ro-

Table 6
Relative energies of ethylideneimine referenced to the trans conformation [a]

trans	cis	N–H rotamer	N–H invertomer	CH_3 rotamer
0.0	1.7	20.8	70.6	0.6 (trans) 1.0 (cis)

[a] kcal/mol units.

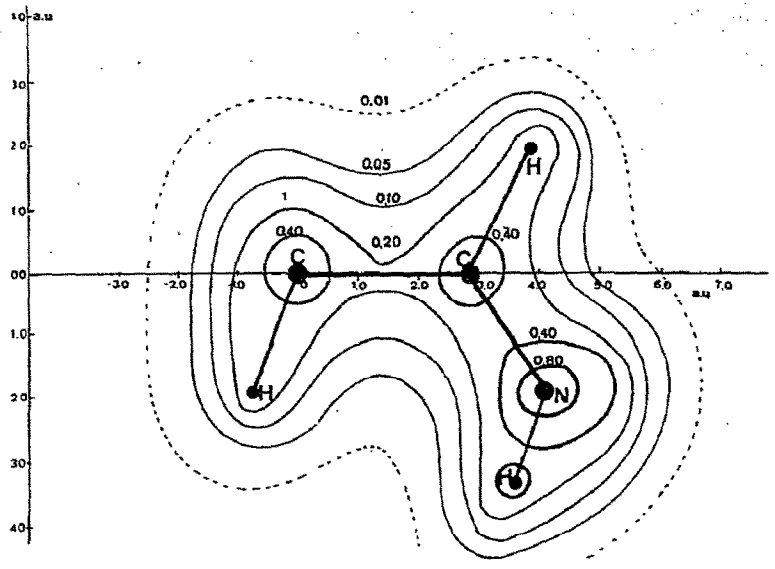

Fig. 11. Trans CH_3CH : NH: Charge contour diagram in the skeletal plane.

tational barriers for the methyl group amount to 0.6 and 1.0 kcal/mol for the t- and c-isomer, respectively. On the other hand the barriers to internal rotation and inversion of the =N—H group are calculated as 70.6 and 20.8 kcal/mol, respectively. The two types of internal motions may therefore be considered as not discernible in most types of spectra, Their barriers are similar in value to those of N-methyl methyleneimine (I) [24], which were found to amount to 23.8 kcal/mol (inversion) and 58.1 kcal/mol (rotation).

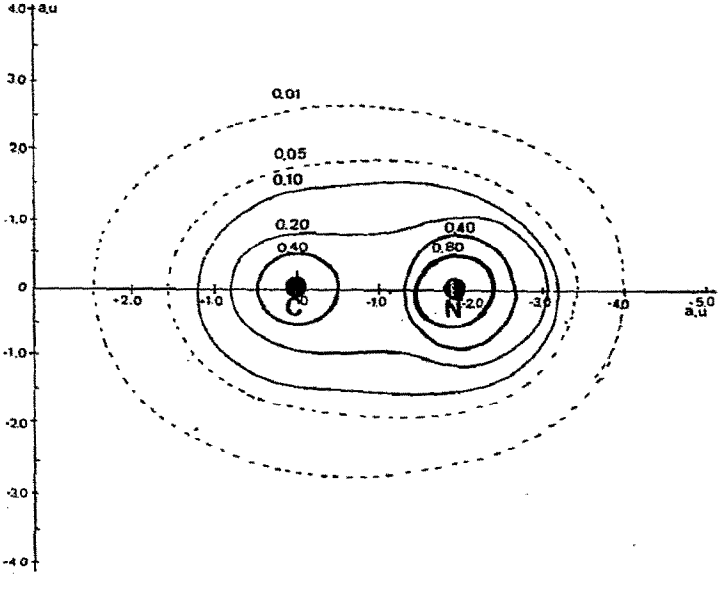

Fig. 12. Trans CH_3CH : NH: Charge density contour diagram in normal plane bisecting the C–N double bond.

Table 7
Comparison of the calculated SCF energies among C_2NH_5 isomers

		E_T [a]	ΔE_T [b]
acetaldimine	trans	−132.8978	0.0
($CH_3CH{=}NH$)	cis	−132.8951	1.7
N-methyiformaldimine		−132.8788	11.9
($CH_2{=}N{-}CH_3$)			
vinylamine		−132.8873	6.6
($CH_2{=}CH{-}NH_2$)			
ethylene imine		−132.8190	49.4
(cyclic CH_2NHCH_2)			

[a] Atomic units. [b] kcal/mol units.

Figs. 11 and 12 represent the charge density contour diagrams in the C—C=N plane and in the plane perpendicular to the skeletal plane passing through the C=N double bond, respectively. They show relatively strong charge localization around the C=N bond (σ and π), which in part is responsible for the high rotational barrier around this axis.

The SCF energy of the experimentally less known ethylidene imine is compared in table 7 with SCF data of experimentally better studied isomers. The SCF energies of the latter have been calculated employing experimental structural parameters derived from microwave spectra, namely $CH_2{:}N{-}CH_3$ [25], $CH_2{:}CH{-}NH_2$ [6] and the cyclic ethylene imine $CH_2\overline{NH}CH_2$ [25]. In this calculations the geometries have not been optimized, so that the corresponding SCF energies might be slightly high. From table 7 one would conclude that the isomers (I), (II) and vinyl amine are qualitatively equally stable. The cyclic imine however has much higher SCF energy than the noncyclic isomers.

5. Discussion

In this section discussion of the experimental results will be devoted to

(i) remarks concerning the catalytic pyrolysis of NTMST and the photolysis of ethylazide; and

(ii) assignment and vibrational analysis of the infrared spectra of isotopic species $CH_3N{:}CH_2$ and $CH_3CH{:}NH$.

5.1. Remarks on pyrolysis and photolysis

5.1.1. Catalytic pyrolysis of NTMST

As has been remarked in section 2 preparation of sufficiently pure gas samples of $CH_3N{:}CH_2$ by pyrolysis of NTMST requires carefully controlled operating conditions, in particular if production of disturning amounts of ammonia is to be suppressed. Under conditions of negligible NH_3 production, the gaseous product still contains traces of NTMST detectable in the matrix spectrum of CH_3NCH_2, cf. fig. 2a. By use of a transport gas and the flow conditions and contact time reported in table 1 it is however possible to arrive at a fairly pure imine. The preparation used earlier [8] apparently leads to unidentified impurities, which gave rise to bands erroneously attributed to $CH_3N{:}CH_2$, cf. section 5.2.

5.1.2. Photolysis of ethylazide

From fig. 5a–c it is evident, that UV irradiation of $CH_3CH_2N_3$: Ar and its d_5 modification induces an irreversible transformation of the azide. The following observations should be stated:

(i) Irradiation effectuates disappearance of the azide spectrum beyond the limit of detection. No bands were observed whose intensity first grew and then decreased as the irradiation time advanced.

(ii) The newly arising spectra appear to be stable against further UV irradiation and are considerably more complex than would be expected for a low symmetry 8-atomic molecule.

From these facts we suppose the photochemical transformation of $CH_3CH_2N_3$ to produce in the Ar matrix at LHe temperature the two long lived particles trans and cis $CH_3CH{:}NH$, in analogy to the photolysis of CH_3N_3 leading to $CH_2{:}NH$ [5].

5.2. Assignment and vibrational analysis

5.2.1. Model calculations of rotational envelopes

Since it has been possible to measure rotational structures of some of the bands in the gas phase spectra of $CH_3N{:}CH_2$, calculation of model envelopes for this molecule proved to be a valuable tool for the assignment. The rotational constants have been determined by microwave spectroscopy of the d_0-modification [25]

$A_0 = 52523.75\ \text{MHz} = 1.751\ \text{cm}^{-1}$,

B_0 = 10666.13 MHz = 0.356 cm^{-1},
C_0 = 9377.19 MHz = 0.313 cm^{-1}.

For calculation of model envelopes the rotational constants of the lower and upper vibrational state were assumed equal and centrifugal distortion was neglected. Furthermore, Boltzmann populations for 298.15 K were assumed and rotational transitions with $J \leqslant 60$ were included, covering a range of ± 70 cm^{-1} centered at the vibrational transition. Typical calculations with slit width of 0.25 cm^{-1} were made by means of a computer program worked out by Pfeiffer [27]. This program allows superposition of A-, B- and C-type envelopes in any ratio and arbitrary (0,0) frequencies. Hybrid bands of any mixing ratio may be simulated. For $CH_3N{:}CH_2$ (A,B)-type hydrbid and C-type envelopes are to be expected. In fig. 3 simulated envelopes (1) are contrasted with observed bands (2) for B, C and (A,B) hybrid type bands.

5.2.2. *Normal coordinate analysis (NCA)*

In order to assist the vibrational assignment of the imines $CH_3N{:}CH_2$, cis and trans $CH_3CH{:}NH$ extended normal coordinate calculations were carried out by means of a computer program published by Hunziker [28]. The calculations were based on

(i) the harmonic force field derived for the molecule $CH_3CH{:}NCH_3$ (trans isomer) [29], serving as a zeroth order approximation in the least squares fitting process;

(ii) the structural parameters of the two types of imines and the internal coordinates associated with them as shown in figs. 13, 14 and tables 8 and 9, respectively; and

(iii) the assumption of covering symmetry C_s neglecting the effects of the internal rotation on the normal modes.

5.2.3. *Assignment*

The results of the assignment of the vibrational spectra of $CH_3N{:}CH_2$, cis and trans $CH_3CH{:}NH$ proposed in this work are collected in tables 2, 3 and 4. Only relevant points will be discussed in some detail.

$CH_3N{:}CH_2$ and $CD_3N{:}CH_2$ – For N-methyl methyleneimine the new assignment is given in table 2 together with the values of the normal frequencies and the approximative composition of the normal modes from group vibrations. A 19-parameter harmonic valence force field comprising 12 different diagonal and 7 off-diagonal constants is given in table 8. Force constants of the latter type were retained if their value equals at least 1.5 times the RMS value. In view of the limited experimental data no attempt has been made to reduce the RMS deviation $\langle \nu_{obs} - \nu_{calc} \rangle$ to less than 10 cm^{-1}. The following comments should be made:

(i) The valence force field resulting from the NCA deviates as a whole only slightly from the force constants transferred from N-methylethylideneimine [29].

(ii) The ν(CH) region exhibits a pronounced Fermi resonance doublet, similar to that reported by Hollenstein et al. [29] consisting of the two matrix bands $2\nu_6(A')$ and $\nu_3(a')$ (2900 cm^{-1}).

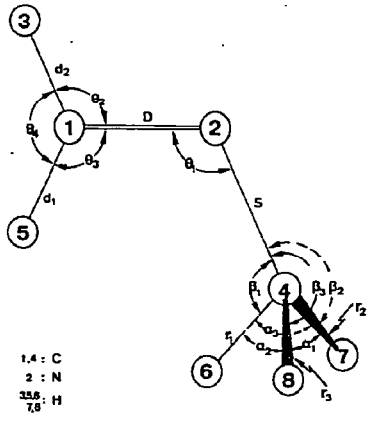

Fig. 13. $CH_3N{:}CH_2$: Structural parametets and internal coordinates.

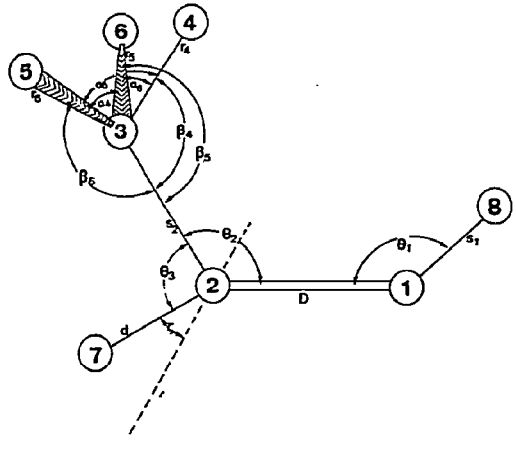

Fig. 14. Trans $CH_3CH{:}NH$: Structural parameters and internal coordinates.

Table 8
$CH_3N:CH_2$ structural parameters, internal coordinates and valence force constants (cf. fig. 13)

Structural [a] parameter	Internal [b] coordinate	Valence force constant (mdyn/Å)
$r_1=r_2=r_3=1.089$ Å	R_1^I,R_2^I,R_3^I	4.678(24)
$d_1=d_2=1.091$ Å	R_4^I,R_5^I	4.783(26)
$D=1.30$ Å	R_6^I	9.567(6)
$S=1.44$ Å	R_7^I	5.191(42)
$\alpha_1=\alpha_2=\alpha_3=109.5°$	$R_8^{II},R_9^{II},R_{10}^{II}$	0.513(9)
$\theta_4=118°$	R_{11}^{II}	0.739(16)
$\beta_1=\beta_2=\beta_3=109.5°$	$R_{12}^{II},R_{13}^{II},R_{14}^{II}$	0.775(21)
$\theta_1=116.9°$	R_{15}^{II}	1.546(72)
$\gamma_{\parallel}$	$R_{16}^{III}(H_{3,5}C_1N_2)$	0.841(43)
$\gamma_{\perp}$	$R_{17}^{IV}(H_{3,5}C_1N_2)$	0.290(7)
τ	$R_{18}^{V}(H_3C_1H_5N_2C_4)$	0.422(21)
τ	$R_{19}^{V}(H_{6,7,8}C_4N_2C_1)$	0.062(7)
	R_6^I,R_4^I	0.328(3)
	R_7^I,R_8^{II}	−0.379(82)
	R_7^I,R_{15}^{II}	0.657(64)
	R_{12}^{II},R_{13}^{II}	−0.025(13)
	R_{15}^{II},R_{12}^{II}	−0.133(62)
	R_6^I,R_{11}^{II}	−0.299(34)
	R_7^I,R_{12}^{II}	0.351(71)

[a] From ref. 27; [b] for definition cf. ref. [12].

(iii) Nearly all a′ normal modes between 1450 and 800 cm^{-1} are strongly composed from several group contributions and therefore cannot be interpreted as simple group vibrations.

(iv) According to the results of this work the assignment of Hinze et al. [8] has to be modified in the following points:

– The matrix absorption bands reported by these authors at 1473, 1045 and 400 cm^{-1} could not be detected with certainty and probably originate from impurities.

– The 2938 cm^{-1} band has been interpreted earlier as $\nu_{as}(CH_3)(a')$. However, it is probably part of the Fermi resonance doublet already mentioned.

– The 2774 cm^{-1} band assigned as $\nu_s(CH_3)(a')$ appears to be too low. Therefore, the latter mode is assigned here to the 2854–2849 cm^{-1} doublet arising probably from matrix effects. On the other hand the 2774 cm^{-1} band appears to be related to a Fermi resonance [29].

– The rotational structure of the 484 cm^{-1} band (cf. fig. 3c) should be considered to have B type contour. This rules out the earlier interpretation as $\rangle C{=}N^-$ torsional mode $\nu_{17}(a'')$ located in this work at 680 cm^{-1} according to its C type band contour. The 464 cm^{-1} band with B type contour should rather be interpreted as $\nu_{12}(a')$ (δ(CNC)).

– For nearly all Ar-matrix bands frequency differences of 2–7 cm^{-1} were found between Hinze et al. [8] and this work. Possibly these and other discrepancies stem from the low M/A ratio used by these authors.

– The matrix spectrum of $CD_3N:CH_2$ published by Hinze et al. [8] is well reproduced by the NCA, resulting in a RMS deviation of 10 cm^{-1}. Similar revisions to those discussed for the (I-d_0) are to be made in the assignment.

$CH_3CH:NH$ and $CD_3CD:ND$ – As has been mentioned in section 5.1.2 the spectra of the photolysis products of ethylazide and its d_5 modification will be considered as superposition of the spectra of the cis isomer

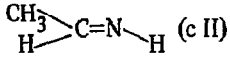
(c II)

and the trans isomer

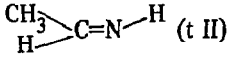
(t II)

and their d_5 modifications, respectively. The analysis of these matrix spectra is rendered more difficult by several uncertainities and therefore cannot be considered as reliable as those of the isomer $CH_3N:CH_2$. This is also expressed by the considerably higher RMS values for calculated vs observed frequencies: 16.6 and 7.5 cm^{-1} for the trans and cis-isomer, respectively. To a large part the 16.6 cm^{-1} value of (t II) results from t$\nu_{15}(a'')$ of the d_5 modification, for which $\nu_{15}^{obs}-\nu_{15}^{calc}\approx 60\ cm^{-1}$ (table 4).

The analysis was based in zeroth order on the valence force fields of $CH_3N:CHCH_3$ [29] and CH_3CHO [30], which proved to reproduce the spectra observed with reasonable accuracy. thereby allowing essentially a discrimination between the two geometrical isomers. The best fit was then searched for by trial and error, leading to the assignment given in table 3 (cis and trans (II-d_0) and in table 4 (II-d_5), respectively.

The following comments appear worthwhile:

(i) Though the ν(NH) stretching mode appears to be

Table 9
CH_3CH:NH structural parameters, internal coordinates and valence force constants (cf. fig. 14)

Structural parameters [a]			Internal coordinates [b]	Force constant	
	cis	trans		cis	trans
S_1	1.016	1.020	R_1^I	5.75(13)	5.891(32)
r_4, r_5, r_6	1.089	1.089	R_2^I, R_3^I, R_4^I	4.767(33)	4.728(23)
d	1.114	1.114	R_5^I	4.692(60)	4.656(29)
D	1.345	1.324	R_6^I	9.11(58)	9.432(16)
S_2	1.54	1.54	R_7^I	5.31(55)	4.92(27)
α_4, α_5, α_6	109.5	109.5	$R_8^{II}, R_9^{II}, R_{10}^{II}$	0.515(11)	0.518(5)
β_4, β_5, β_6	109.5	109.5	$R_{11}^{II}, R_{12}^{II}, R_{13}^{II}$	0.670(25)	0.638(15)
θ_1	113	247	R_{14}^{II}	0.627(40)	0.705(5)
ζ	0.5		R_{15}^{III}	1.039(95)	0.862(42)
γ_1			$R_{16}^{IV}(H_7C_2N_1C_3)$	0.308(25)	0.240(11)
θ_2	124	124	R_{17}^{II}	1.58(32)	1.916(10)
τ			$R_{18}^{V}(N_1C_2C_3H_{7,8})$	0.454(28)	0.463(8)
τ			$R_{19}^{V}(N_1C_2C_3H_{4,5,6})$ $(H_7C_2C_3H_{4,5,6})$	0.05	0.05
			R_2^I, R_3^I		0.147(49)
			R_7^I, R_8^{II}	−0.28(18)	−0.241(30)
			R_7^I, R_{15}^{III}		−0.668(85)
			R_8^{II}, R_{12}^{II}		0.022(9)
			$R_{17}^{II}, R_{15}^{III}$		−0.488(47)
			R_{11}^{II}, R_{17}^{II}	−0.31(17)	
			R_1^I, R_6^I	−1.37(46)	

[a] Bond length in Å, bond angles in degrees, values used for *ab initio* calculation, for definition see fig. 13 and section 4.
[b] For definition cf. ref. [12] and fig. 13.

very weak in related molecules CH_3N:NH [31], CH_2:NH [5] considerable effort has been made to detect this mode. Use of ordinate expansion (30X) finally yielded reproducibly the spectra in figs. 6 and 9, respectively, which support rather definitely the presence of ν(NH) and ν(ND) bands. For (II-d_0) 3 bands in the range 3300–3200 cm^{-1} are observed, which have been attributed to $t\tilde{\nu}_1$(NH)(a') (3264 cm^{-1}), $c\tilde{\nu}_1$(NH)(a') (3247 cm^{-1}) and to $c2\tilde{\nu}_5$ (a') (3288 cm^{-1}). For (II-d_5) the same region exhibits a single band near 3317 cm^{-1} of unknown origin, but it may be interpreted as a combination tone. In the 2500–2400 cm^{-1} region two bands are observed at 2452 cm^{-1}, $t\tilde{\nu}_1$ (a') and 2425 cm^{-1}, $c\tilde{\nu}_1$ (a'), which may be considered as ν(ND) modes.

(ii) The ν(CH) – ν(CD) isotope shifts behave similarly to related molecules like CH_3CH:NCH_3 [29], CH_3CHO [30].

(iii) The ν(C:N)-region of (II-d_5) exhibits 6 bands, which may be grouped into site doublets at 1631/1628 and 1615/1613 cm^{-1} attributed to the fundamentals $c\nu_5$(a'), $t\nu_5$(a') and to combination bands, respectively.

Table 10
Molecular data of C_2-imines, required for statistical thermodynamic functions

Quantity	cis-CH_3CH:NH	trans-CH_3CH:NH	CH_3N:CH_2
M (g/mol)	43.042		
I_a (uÅ^2)	9.51545 [a]	10.19478 [a]	9.6248 [b]
I_b (uÅ^2)	51.6002	51.15199	47.3959
I_c (uÅ^2)	58.0990	58.44187	53.9107
σ	1	1	1
$10^{40} I_\alpha$ (g cm^2)	5.3	5.3	5.24
I_α (uÅ^2)	3.20	3.20	3.164 [b]
λ_a	0.930 [c]	0.916 [c]	0.867
λ_b	0.368	0.401	0.496
λ_c	0	0	0
$10^{40} I_{red}$ (g cm^2)	4.786	4.730	4.546
I_{red} (uÅ^2)	2.89	2.85	2.74
V_3 (cal/mol)	1000 [d]	600 [d]	1970 [b]

[a] Ref. [6].
[b] Ref. [27].
[c] Calculated from standard geometrical parameters.
[d] Quantum chemical values, cf. table 6.

As table 4 shows there exist several possibilities for Fermi resonance. An attempt has been made to analyse these resonances but no decision between various interpretations seems possible; table 4 gives one of these [12].

(iv) Among the assignments of the fingerprint bands a pronounced discrepancy for the band near 986 cm^{-1} of (II-d_5) should be mentioned. If force constants are required to deviate but slightly from those of related molecules the differences between calculated and observed frequencies for this absorption could not be reduced to less than 60 cm^{-1}. Its assignment to tν_{15}(a″) should be considered as a compromise.

6. Chemical thermodynamic data of N-methylmethylenimine and ethylidine imine

In this section tables of conventional thermodynamic functions of the imines treated in this work as calculated in the ideal gas-rigid rotor-harmonic oscillator – hindered internal symmetric rotor-approximation will be presented. For convenience the basic molecular data are collected in table 10. Therefrom and from the fundamental frequencies listed in tables 2 and 3 thermodynamic functions as tabulated in tables 11, 12 and 13 were calculated [32], using values of the fundamental physical constants published by IUPAC [33]. Further chemical thermodynamic data may be obtained, if thermochemical information is included. Since no calorimetric measurements

Table 11
Ideal gas thermodynamical functions of cis-ethylideneimine (JK^{-1} mol^{-1}) [a]

T (K)	$-(G^0-H_0^0)/T$	$(H^0-H_0^0)/T$	S^0	C_p^0
298.15	222.50	43.72	266.52	57.32
300	222.76	43.76	266.86	57.53
400	236.14	48.61	284.00	71.16
500	247.68	54.31	302.62	84.20
600	258.26	60.27	319.00	95.50
700	267.92	66.03	334.46	105.54
800	277.28	71.52	349.14	114.04
900	286.02	76.63	363.00	121.38
1000	294.40	81.43	376.13	127.73

[a] Based on fundamentals of cCH$_3$CH:NH.

Table 12
Ideal gas thermodynamical functions of trans-ethylideneimine (JK^{-1} mol^{-1}) [a]

T (K)	$-(G^0-H_0^0)/T$	$(H^0-H_0^0)/T$	S^0	C_p^0
298.15	223.94	43.45	267.40	56.96
300	224.20	43.53	267.74	57.21
400	237.44	48.38	285.79	70.17
500	248.86	54.04	302.87	83.40
600	259.21	59.93	319.14	94.92
700	268.88	65.61	334.50	113.44
800	278.03	71.04	349.08	104.87
900	286.67	76.18	362.86	120.88
1000	294.98	80.93	375.92	127.29

[a] Based on fundamental frequencies of $tCH_3CH:NH$.

Table 13
Ideal gas thermodynamical functions of N-methylmethylenimine (JK^{-1} mol^{-1}) [a]

T (K)	$-(G^0-H_0^0)/T$	$(H^0-H_0^0)/T$	S^0	C_p^0
298.15	219.41	44.19	263.07	59.88
300	219.67	44.31	263.41	60.14
400	233.25	49.82	283.06	73.26
500	244.92	55.43	300.76	85.82
600	255.80	61.05	317.39	96.85
700	265.76	66.81	333.03	106.50
800	275.15	72.29	347.82	114.88
900	283.98	77.49	361.81	122.18
1000	292.39	82.31	375.04	128.55

[a] Based on fundamental frequencies of $CH_3N:CH_2$: Ar.

have yet been made on these imines, one may refer to the SCF ground state energies reported in section 4. It should be pointed out however, that use of quantum chemically calculated thermochemical values may introduce considerable systematic errors and therefore should be considered with caution.

In table 14 values of chemical thermodynamic data are collected based on the SCF quantum chemical ground state energies given above. Apparently the required empirical group contributions are not known, so that the quantum chemical values cannot be contrasted with empirical estimates [34].

Furthermore, the quantum chemical SCF ground state energies allow calculation of the equilibrium constant of the reactions

$$\text{-t-}CH_3CH{:}NH + CH_3N{:}CH_2 = 0, \quad (3)$$

$$\text{-t-}CH_3CH{:}NH + \text{c-}CH_3CH{:}NH = 0. \quad (4)$$

For the reaction effects only differences of SCF ground state energies are required, so that systematic errors may be somewhat less serious. Since only partially optimized SCF energies were available in this work, systematic errors may nevertheless be significant. Numer-

Table 14
Chemical thermodynamic values for interconversion of C_2-imines

T (K)	$-t(II) + c(II) = 0$ (3) [a] $\Delta H^0(T)$ (J mol^{-1})	$\Delta G^0(T)$ (J mol^{-1})	K_3	$-t(II) + (I) = 0$ [b] $\Delta G^0(T)$ (J mol^{-1})	$\Delta G^0(T)$ (J mol^{-1})	K_4
298.15	5988.90	6419.16	0.075	48046.12	49176.01	2.4×10^{-9}
300	6070.04	6421.69	0.076	48060.42	49169.55	2.7×10^{-9}
400	6078.42	6506.84	0.14	48403.14	49503.15	3.4×10^{-7}
500	6122.58	6581.14	0.21	48521.24	49811.32	6.3×10^{-6}
600	6196.72	6556.42	0.27	48499.84	49873.81	4.6×10^{-5}
800	6370.86	6598.11	0.37	48826.84	50142.36	5.3×10^{-4}
1000	6487.73	6571.67	0.45	49203.59	50420.46	2.3×10^{-3}

[a] $\Delta E_T = \Sigma_i \nu_i E_{Ti} = 6826.30$ J mol^{-1}. [b] $\Delta E_T = 49884.50$ J mol^{-1}.

ical values for the equilibrium constants K_3 and K_4 are tabulated in table 14. They may be valuable in further attempts to produce the primary imine thermal reactions.

It clearly shows that under the conditions of thermal equilibrium quantum chemical SCF energies would predict mainly production of the primary imines.

Acknowledgement

The authors wish to express their gratitude for financial support to the Swiss National Foundation (Project Nos. 2.808.0-73 and 2.110.0-74) and to Messrs. Sandoz AG, Basle. Furthermore, we wish to thank Drs. R. Meyer, H. Hollenstein, and H. Kühne for valuable advice and technical support, and the ETHZ Computing Center for a generous free grant of computing time.

References

[1] S. Patai, ed., The Chemistry of the Carbon–Nitrogen Double Bond (Interscience, New York, 1970) p. 149.
[2] D.E. Milligan, J. Chem. Phys. 35 (1961) 1491.
[3] C.B. Moore, G.C. Pimentel and T.D. Goldfarb, J. Chem. Phys. 43 (1965) 63.
[4] D.R. Johnson and F.J. Lovas, Chem. Phys. Letters 15 (1972) 65.
[5] M.E. Jacox and D.E. Milligan, J. Mol. Spectr. 56 (1975) 333.
[6] F. Lovas, F.O. Clark and E. Tieman, 5th Austin Symposium on Gas Phase Molecular Structure (1974).
[7] P.D. Godfrey, R.D. Brown, B.J. Robinson and M.W. Sinclair, Atrophys. Letters 12 (1973) 119.
[8] J. Hinze and R.F. Curl Jr., J. Am. Chem. Soc. 86 (1964) 5068.
[9] J. Meier, F. Akermann and Hs.H. Günthard, Helv. Chim. Acta 51 (1968) 1686.
[10] J.L. Anderson, US patent 272 (1956) 9679.
[11] B.G. Gowenlocke, K.E. Thomas, J. Chem. Soc. B, Phys. Org. (1966) 409.
[12] I. Stolkin, Thesis Nr. 5616, ETH Zürich (1975).
[13] Beilstein's Handbuch der Organischen Chemie. Vol. 26 (1944) 1.
[14] H. Staudinger and E. Hauser, Helv. Chim. Acta (1921) 872.
[15] R.D. Werder, Thesis No. 3970, ETH Zürich (1967).
[16] P. Groner, I. Stolkin and Hs.H. Günthard, J. Phys. E, Sci. Instr. 3 (1970) 261.
[17] J.L. Whitten, J. Chem. Phys. 44 (1966) 359.
[18] J.L. Whitten, J. Chem. Phys. 39 (1963) 349.
[19] T.-K. Ha, J. Mol. Struct. 12 (1972) 171.
[20] T.-K. Ha, J. Mol. Struct. 21 (1974) 753.
[21] T.-K. Ha, E. Mathier and Hs.H. Günthard, to be published.
[22] T.-K. Ha, H. Frei, R. Meyer and Hs.H. Günthard, Theor. Chim. Acta 34 (1974) 277.
[23] R. Meyer, T.-K. Ha, H. Frei and Hs. H. Günthard, Chem. Phys. 9 (1975) 393.
[24] G. Merenyi, G. Wettermark and B. Ross, Chem. Phys. 1 (1973) 340.
[25] K.V.L.N. Sastry and R.F. Curl Jr., J. Chem. Phys. 41 (1964) 77.
[26] B. Bak and S. Skaarup, J. Mol. Struct. 10 (1971) 385.
[27] F. Pfeiffer, Diploma Thesis, ETH Zürich (1966).
[28] H. Hunziker, J. Mol. Spectrosc. 17 (1965) 131.
[29] H. Hollenstein and Hs.H. Günthard, Chem. Phys. 4 (1974) 368.
[30] H. Hollenstein and Hs.H. Günthard, Spectrochim. Acta 27A (1971) 2027.
[31] M.N. Ackermann, J.J. Burdge, N.C. Craig, J. Chem. Phys. 58 (1973) 203.
[32] L.N. Godnew, Berechnung thermochemischer Funktionen aus Molekuldaten (VEB, Berlin, 1963).
[33] IUPAC Information Bulletin Nr. 32 (1968) 38.
[34] S.W. Benson, Thermochemical Kinetics (Wiley, New York, 1968).